

Horizontal velocity of Saturn's polar regions and Hexagon

A. Antuñano¹, T. del Rio-Gaztelurrutia^{1,2}, A. Sanchez-Lavega^{1,2}, and R. Hueso^{1,2}

¹ Departamento de Física Aplicada I, E. T. S., Ingeniería, Universidad del País Vasco. Alameda Urquijo s/n, 48013 Bilbao, Spain

² Unidad Asociada Grupo Ciencias Planetarias UPV/EHU-IAA(CSIC), Spain

Abstract

We study the horizontal velocity and vorticity field of Saturn's polar regions (from 60° to 90° North and South) by analyzing data retrieved by Cassini's Imaging Science System instrument. We determine the zonal mean profiles for the North and South up to 89.5°S and 89.9°N and we also build two dimensional zonal and meridional velocity maps that allow to compute vorticity maps. The hexagonal feature encloses an eastward jet at 75.8°N that becomes non-zonal. The peak of this eastward jet lies closer to the pole than the eastward jet in the south, which is zonal. A similar anticyclone to the North Polar Spot (NPS) that was observed by the Voyagers in 1981 is observed in the South on 2008–2009 images impinging on the eastward jet. However, it seems that this vortex does not excite a wave on its closest jet stream. Finally, we study the stability of the zonal jets North and South, where we find potential instabilities at the flank of these jets.

1 Introduction

Images obtained by Voyager flybys in 1980 and 1981 showed an hexagonal feature in Saturn's North pole at 75° planetocentric latitude enclosing a fast eastward jet with a velocity peak of 120 m s^{-1} [7] and a large anticyclone denotated North Polar Spot (NPS) [13]. These same features and the eastward jet were reobserved by ground-based telescopes and with Hubble Space Telescope (HST) during 1990–1995 [12, 3]. During 1997 and 2002 images captured by HST showed a fast eastward jet in the South pole of Saturn [14]. However, these images did not showed an hexagonal feature, nor a large anticyclone in the South polar region. After Cassini's arrival to Saturn in 2004, the Hexagon an the eastward jet were again observed, first by VIMS instrument when the North pole was in Saturn's night [2] and then by ISS

instrument, after Saturn's equinox in 2009. However, the NPS was not longer present in these images. During this epoch, the south polar region was also observed and the images showed a fast zonal eastward jet at latitudes similar to that in the North. This had already been observed in images in the thermal infrared obtained from Earth [9], and they also showed a polar vortex [15] with a dark eye surrounded by fast white clouds [4]. Once Saturn's North pole was illuminated by sunlight, images captured by ISS instrument showed a similar polar vortex in the North pole. As these polar vortices on the giant planets is operate under a very different thermo-chemical conditions, it is of great interest to study these polar vortices for planetary comparison. Here we use images obtained by the Wide Angle Camera (WAC) and by the Narrow Angle Camera (NAC) of Cassini ISS with the aim of comparing the morphology of both polar regions from 60° to 90° North and South and obtaining wind and vorticity maps.

2 Image selection, navigation and measurement methods

In this study we have used images captured by the WAC and the NAC of the Imaging Science System onboard the Cassini spacecraft. We have used 8 WAC images and 4 NAC images from June 2013, for the study of the North polar region, and 9 WAC images from October 2006 and December 2008 and 2 NAC images from July 2008, for the study of the South polar region. We have used CB2 or CB3 narrow filtered images (centered at 752 nm and 939 nm respectively) [11] because they reveal the features at the top of the ammonia clouds at around 350–750 mbar altitude [10, 15, 6] with the highest contrast. All NAC images were used to study the polar vortices while the WAC images where used to measure winds for latitudes greater than 60° North and South.

All these images have been navigated using PLIA software [8]. This software allows a manual correction of the navigation by limb fitting and/or adjusting the pole and it uses information extracted from SPICE kernels [1]. Once the navigation is performed WAC images are polar projected from 60° to 90° North and South and NAC images are polar projected from 85° to 90° using an azimuthal equidistant projection [18] in both cases.

Assuming that the clouds are passive tracers, we have used two different methods to measure wind vectors: a) A bidimensional brightness correlator that allows us to validate, correct or ignore wind vectors [8] used for image pairs separated by a maximum of 120 minutes and b) Cloud tracking used for the measurements of the wind vectors of NAC images near the pole separated by 40–80 minutes as the clouds move fast and change morphology rapidly. The amount of wind vectors obtained by this second method is only 1% of the total measurements.

There are different sources of errors: a) An error introduced by the resolution limit and the time interval of the image pairs, which varies from 4 m s^{-1} to 8 m s^{-1} for the WAC images used to measure the South polar region and around 10 m s^{-1} for the WAC images used to measure the North. NAC images error is less than 1 m s^{-1} for both cases; b) The navigation uncertainty for the WAC images is of a half a pixel and as large as ten pixels for NAC images. This navigation error is of the order of the error introduced by the resolution and time interval limit.

3 Results

3.1 Morphology

Figure 1 shows both Saturn's polar regions which present many similarities. Puffy clouds of similar sizes and form are present all over both polar regions. A fast eastward jet is also present in both poles with similar velocity peak. However, these eastward jets are of different shape, the one in the North is an Hexagon [7] [12] [3] and the other is circular, and are located at different latitudes, being the Hexagon closer to the pole (75.8°N vs 70.4°S). The NPS from Voyager epoch is not present in the North in Cassini images, however, there is a very similar anticyclone in the South polar regions in Cassini images from April 2008 to January 2009, which we denote South Polar Spot (SPS). A polar vortex extending from 88.5° to 90° North and South [15, 5, 17] is also present in both hemispheres.

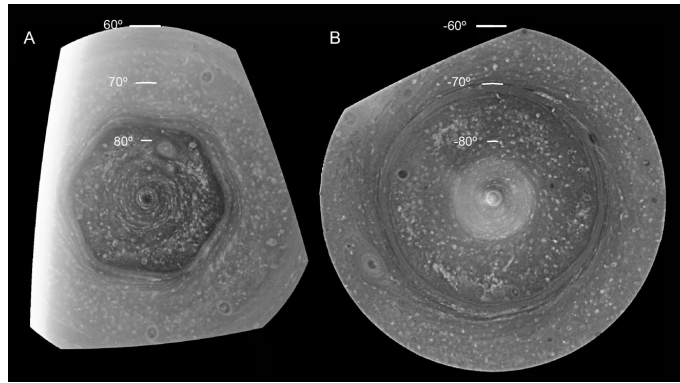


Figure 1: Panels A and B show a polar projection from 60° to 90° North and South respectively, captured on 14 June 2013 with CB2 filter for panel A and on 3 December 2008 with CB2 filter for panel B.

3.2 Wind maps and Zonal Wind Profile

In this study we obtained the zonal and meridional velocity maps and the zonal mean velocity profile up to 89.9° North and South. As it can be seen in Fig. 2 the zonal velocity maps are very similar in both hemispheres, reaching velocities of around $100\text{--}120\text{ m s}^{-1}$ in both eastward jets and $140\text{--}160\text{ m s}^{-1}$ in both polar jets. Meridional velocity maps of the North and South are very different. In the North polar region meridional velocities from 20 m s^{-1} to -20 m s^{-1} are observed in the hexagonal jet. However, there is no significant meridional wind in the South polar region as expected for a zonal jet.

3.3 Vorticity maps

From the zonal and meridional velocities measured, we have extracted the vorticity maps of both polar regions (Fig. 3). In this case, we have calculated the vertical component of the

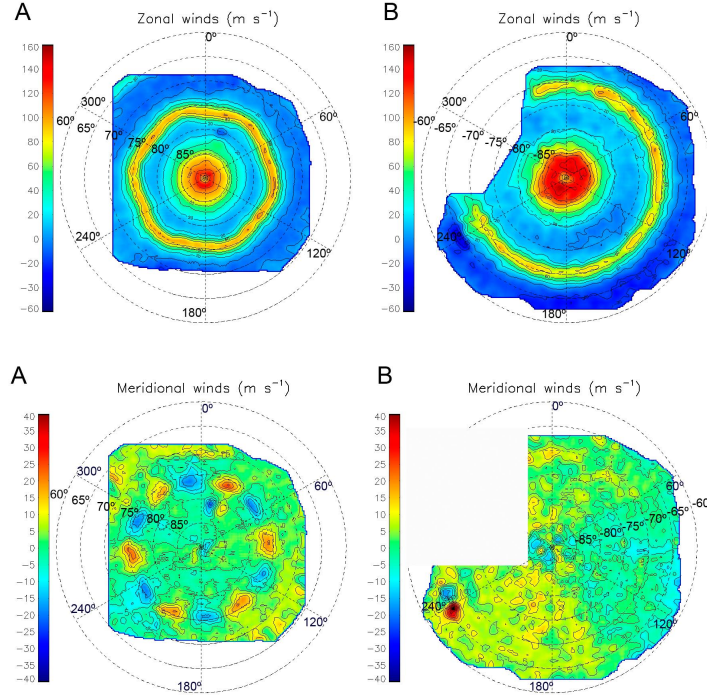


Figure 2: *Top*: Panels A and B show the zonal velocity maps averaged over all epoch of observation of the North and South respectively. *Bottom*: Panels A and B show the meridional velocity maps averaged over all epoch of observation of the North and South respectively.

relative vorticity, which estimates the value of the potential vorticity and is given by [16]:

$$\zeta(\lambda, \varphi) = \frac{1}{R \cos \varphi} \frac{\partial v}{\partial \lambda} - \frac{1}{R} \frac{\partial u}{\partial \varphi} + \frac{u}{R} \tan \varphi, \quad (1)$$

where u and v are zonal and meridional velocities respectively, R is the radius of the planet at that latitude, φ is the latitude and λ is the longitude. The results showed that the vorticity peaks of the eastward jet in North and in the South are of order $6 \pm 1 \times 10^{-5} \text{ s}^{-1}$, a tenth of the Coriolis parameter. However, as we move to the pole, the geometric term $\frac{u}{R} \tan \varphi$ of eq. 1 grows in magnitude and the vorticity reaches values of the Coriolis parameter in the polar jets $-25 \pm 1 \times 10^{-5} \text{ s}^{-1}$ at 89.9°N .

3.4 Vorticity gradients

We have analysed the Rayleigh-Kuo instability criterion for barotropic atmospheres in the eastward jets. The instability criterion is satisfied whenever $\frac{\partial^2 u}{\partial^2 y} > 0$.

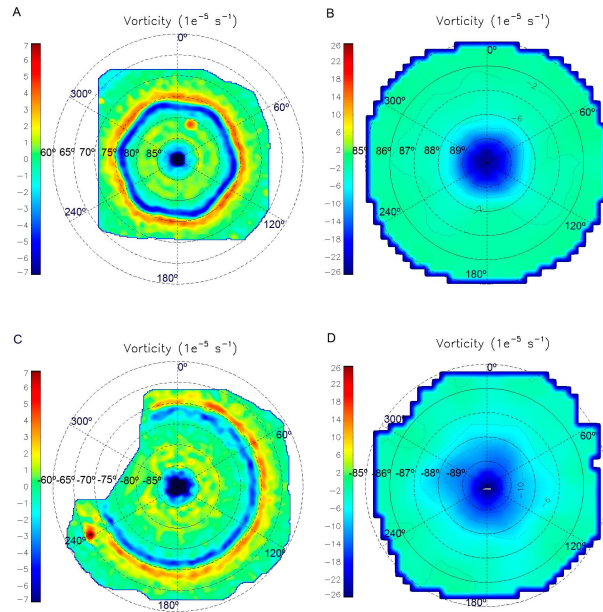


Figure 3: Panels A and C show the vorticity maps from 60° to 83° North and South respectively. Panels B and D show the vorticity maps from 83° to 90° North and South respectively.

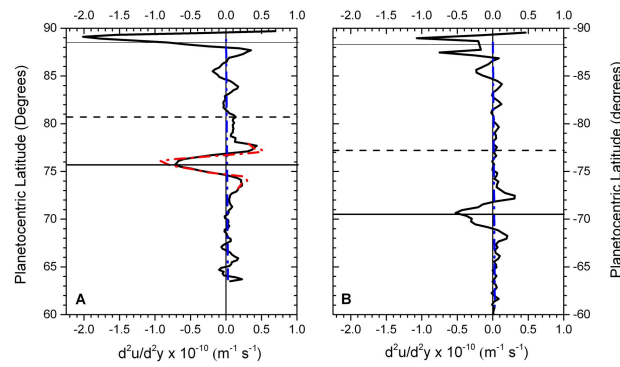


Figure 4: Vorticity gradients of the North (panel A) and South (panel B) are represented by the black solid line. The beta parameter is represented by the blue dashed line and the horizontal dashed lines represent the westward jets while the horizontal solid lines represent the eastward jets. The red dashed line represents the meridional vorticity gradient taking into account the meandering effect of the hexagon.

As Fig. 4 shows, the beta parameter is much smaller than the ambient vorticity at latitudes close to the eastward jets and then, the Rayleigh-Kuo instability is satisfied at the two flanks of the eastward jets.

Acknowledgments

We gratefully acknowledge the work of the Cassini ISS team that allowed these data to be obtained. A.A. is supported by a MINECO FPI PhD Studentship. This work was supported by the Spanish project AYA2012-36666 with FEDER support, PRICI-S2009/ESP-1496, Grupos Gobierno Vasco IT-765-13 and by Universidad del País Vasco UPV/EHU through program UFI11/55.

References

- [1] Acton, C. H. 1996, *Planetary and Space Science*, 44, 65
- [2] Baines, K. H., Momary, T. W., Fletcher L. N. et al. 2007, *Planetary and Space Science*, 57, 1671
- [3] Caldwell, J., Hua, X-M., Turgeon, B., Westphal, J. A., & Barnet, C. D. 1993, *Science*, 260, 326
- [4] Dyudina, U. A., Ingersoll, A. P., Ewald S. P. et al. 2008, *Science*, 319, 1801
- [5] Dyudina, U. A., Ingersoll, A. P., Ewald S. P. et al. 2009, *Icarus*, 226, 1020
- [6] García-Melendo, E., Sánchez-Lavega, A., Rojas, J. F., Pérez-Hoyos, S., & Hueso, R. 2009, *Icarus*, 201, 818
- [7] Godfrey, D. A. 1988, *Icarus*, 76, 335
- [8] Hueso, R., Legarreta, J., García-Melendo, E., Sánchez-Lavega, A. & Pérez-Hoyos, S. 2009, *Icarus*, 203, 499
- [9] Orton, G. S. & Yanamandra-Fisher, P. A. 2005, *Science*, 307, 696
- [10] Pérez-Hoyos, S., Sánchez-Lavega, A., French, R. G. & Rojas, J. F. 2005, *Icarus*, 176, 155
- [11] Porco, C. C., West, R. A., Squyres, S. et al. 2004, *Space Science Reviews*, 115, 363
- [12] Sánchez-Lavega, A., Lecacheux, J., Colas, F. & Laques, P. 1993, *Science*, 260, 329
- [13] Sánchez Lavega A., Rojas, J. F., Acarreta, J. R. et al. 1997, *Icarus*, 128, 322
- [14] Sánchez-Lavega, A., Prez-Hoyos, S., Acarreta, J. R. & French, R. G. *Icarus*, 160, 216
- [15] Sánchez-Lavega, A., Hueso, R., Pérez-Hoyos, S. & Rojas, J. F. 2006, *Icarus*, 184, 524
- [16] Sánchez-Lavega, A. 2011b, CRC Press, Boca Raton, Fla.
- [17] Sayanagi, K. M., Ewald, S. P., Dyudina, U. A., & Ingersoll, A. P. 2013b, AAS/Division for Planetary Sciences Meeting Abstracts, 45, #509.06
- [18] Snyder, J. P. 1987, U. S. Geological Survey Professional Paper 1395 (Washington, DC: U. S. Government Printing Office), 191